HOT JET AND MACH NUMBER EFFECTS ON
JET INTERACTION UPSTREAM SEPARATION

Douglas J. Hudson*, James W. Trolier†, Thomas B. Harris‡
Science Applications International Corporation
Wayne, PA 19087

Abstract

Computational fluid dynamics solutions have been performed to evaluate flowfield separation effects resulting from the firing of a divert thruster on a biconic endoatmospheric interceptor. Comparisons are made with cold jet wind tunnel data in order to validate the prediction model which is then applied to hot jet flight conditions at a higher Mach number and momentum flux ratio. Scaling of the wind tunnel results to flight based on momentum flux ratio implies the existence of a large separated region onto the interceptor forecone. Simulation results for the hot jet, however, showed no separation onto the forecone. The reasons for these differences are primarily attributed to the higher freestream Mach number and lower specific heat ratio in the hot jet case. Other issues concerning the scaling of cold jet wind tunnel results to flight are also discussed.

Introduction

Many endoatmospheric interceptor designs employ divert thrusters located near the vehicle center-of-gravity for enhanced maneuverability and lethality in the end game homing process. The interaction of the divert jet with the oncoming supersonic or hypersonic flowfield creates a complicated three dimensional flow structure which includes flow separation as well as a number of strong shocks and expansions. The changes in the flowfield which result from this type of jet interaction can have a large impact on overall interceptor performance.

Changes in the surface pressure distribution about the interceptor due to jet interaction can cause either amplification or deamplification of the basic jet thrust. In some extreme cases, complete reversal of the intended control force has been observed. A thorough understanding of the force and moment amplification/deamplification resulting from jet interaction can be of extreme importance for accurate simulation of interceptor response to control inputs, especially at low altitudes. Jet interaction force and moment amplification effects are highly configuration dependent and have been examined in a number of studies.[1-8]

Another area of concern to interceptor designers related to jet interaction is augmented local surface heating resulting from the jet-induced separation shocks. Understanding of this phenomenon is especially important for thermal protection system design in applications which utilize solid propellant motors since, for such systems, the divert motor fires continuously once it is engaged.

The last major difficulty caused by jet interaction, and the motivation for this study, is the influence of the divert thruster on interceptor sensor performance. A rough schematic of a high altitude jet interaction flowfield and its potential effect on sensor performance is shown in Figure 1 for a forward-looking interceptor design.

As interceptor altitude and/or thrust level increases, the region of separation introduced upstream of the divert jet generally moves further toward the vehicle nose. Under some conditions, such as those illustrated, the separated region can cover all or part of a forward-looking sensor window, such as one mounted on the vehicle forecone.

The presence of this separated region over the sensor window induces a number of aero-optic effects which can degrade sensor performance. Some of these include additional boresight error from the mean

---

* Staff Scientist, Member

† Technical Director, Member

‡ Division Manager & Vice President, Member

19981123 133

density gradients across the jet layer, IR radiance emitted by the hot jet gases (such as CO_2, H_2O, and CO) or particulates in the field-of-view, and blur and jitter resulting from flowfield unsteadiness and jet-induced turbulent density fluctuations. In addition, augmented local heating caused by the jet separation shock can cause thermo-structural distortion of the sensor window which can, in turn, distort the incoming images.

In order to evaluate the impact, if any, which these effects have on sensor performance, it is first necessary to determine the extent and properties of the separated region upstream of the jet. The remainder of this paper focuses on the requirements for accurate evaluation of jet-induced separation effects in the endoatmospheric interceptor flight environment.

One approach to evaluating jet interaction effects for a given interceptor design is to test a subscale model of the configuration in a wind tunnel or shock tunnel and scale the results to flight. This approach is commonly used for evaluating jet interaction force and moment amplification effects.[3, 6, 8] However, due to limits on program resources and ground test facility capabilities, it is not usually possible or practical to test at the actual freestream or jet gas conditions which will be encountered in flight.

As a result, jet interaction tests are often performed using a cold gas at tunnel conditions which match a subset of the desired flight parameters (Mach number, Reynolds number, jet-to-freestream mass or momentum flux ratio, etc.). The data obtained is then correlated versus a parameter such as mass or momentum ratio and these correlations are then used to determine expected flight performance. If the predictions are strongly sensitive to changes in any of the parameters not simulated in the tunnel, large uncertainties in expected flight performance can result.

Because of the complexity of jet interaction flowfields, they have stretched the limits of simple analytical models. However, with the development of modern robust CFD (computational fluid dynamics) algorithms and high-speed supercomputers, high fidelity computational analysis (3-D Navier-Stokes) of jet interaction flowfields is possible, but can still be quite costly. In addition, it is necessary to adequately validate computational models to gain confidence in the accuracy of their predictions.

Motivation

The motivation for the current study was to evaluate and identify altitude regimes where jet-induced separation could degrade sensor performance for a biconic interceptor flying at boosted velocities (> 3 km/s). It was desired to take an existing concept designed for lower speed intercepts and see how it would perform under higher velocity conditions with only minimal changes to the original design. In addition to the higher velocity flight conditions, limitations were also placed on the allowable angle-of-attack range
($-4° < \alpha < +4°$) due to sensor field-of-view considerations.

Mach 8 jet interaction wind tunnel tests for the original design showed the presence of massive separation onto the vehicle forecone under some conditions. Force and moment tests for this same configuration found that the jet force and moment amplification factors correlated well with the jet-to-freestream momentum ratio. Predictions of flight performance were then made by scaling the correlated wind tunnel data to flight velocities and altitudes at equivalent momentum flux ratios.

Using this same type of logic, estimates of boosted velocity jet-induced separation extent were made by scaling the measured wind tunnel separation distances to flight conditions at equivalent momentum flux ratios. Based on these estimates, the boosted velocity interceptor could experience large amounts of flow separation over the vehicle sensor window for altitudes on the order of 50-55 km. In order to ascertain the accuracy of these estimates and their potential impact on interceptor performance, it was decided to perform a series of CFD solutions. These solutions would be performed at altitudes beginning at 65 km and descending in increments of 5-10 km until no separation was observed over the sensor window. These solutions would then provide a means of bounding where separation could be expected over the sensor window. In addition, each solution would also provide a means of predicting what aero-optic effects would result under the particular conditions of interest.

Approach

The CFD code used for this investigation is a modified version of the GASP 2.0 (General Aerodynamic Simulation Program) developed by Walters, et. al.[9] GASP 2.0 is a 3-D multi-block CFD

code which solves the Reynolds-averaged Navier-Stokes equations and their subsets (Euler, Thin-Layer and Parabolized Navier-Stokes). It has a wide range of capabilities including implicit, finite-volume, upwind solution algorithms, fully coupled nonequilibrium thermodynamics and chemistry, zonal grid methods, and advanced turbulence modeling. SAIC maintains several custom versions of GASP 2.0 which includes additions such as a two-phase flow capability, additional solution algorithms and chemistry models, surface material ablation boundary conditions, and enhancements to the baseline code's turbulence models.

The equation set solved in this study are the laminar Navier-Stokes equations. The vehicle boundary layer and jet mixing are assumed to be laminar in this study because of the low Reynolds numbers (high altitudes) involved and also to maximize the predicted separation extent. This was done to provide a conservative upper bound on the altitude regime where separation effects are important.

The inviscid fluxes are modeled using first or second-order accurate upwind schemes - Van Leer's flux vector splitting in the circumferential direction and Roe's flux difference splitting in the axial and normal directions. Using Van Leer's flux vector splitting in the circumferential coordinate direction has been found to add additional robustness to the solution procedure without causing additional .smearing of the viscous layer. Viscous flux terms are evaluated using standard central differences.

Boundary conditions applied to the computational domain include fixed supersonic inflow conditions for the freestream (outer) boundary and jet inflow; constant temperature, no slip, and zero normal pressure gradie. t on the vehicle surface; and simple zeroth order-extrapolation at the interceptor base plane (outflow) boundary.

The solution is advanced in time using a two factor approximate factorization scheme in the crossflow plane with Gauss-Seidel-type relaxation in the streamwise direction. One iteration is considered to consist of a single forward and a single backward Gauss-Seidel sweep. In addition, five levels of grid sequencing and local time stepping are used to accelerate solution convergence to a steady-state. Approximately 1500-2000 iterations and 100-120 CPU hours on a CRAY EL-98 are required to obtain a solution.

As noted in Reference 5, the overall residual for jet interaction computations is typically reduced by only 2-3 orders of magnitude before it begins to oscillate, typically before a solution has completely stabilized. This behavior can occur for a variety of reasons including basic unsteadiness in the separated flowfield, numerical oscillations introduced by local time stepping, or "hard" numerical switches such as the minmod limiter often employed with upwind schemes. As such, other means of determining convergence must be used.

For this study, convergence is determined by monitoring the relative change in the vehicle surface pressure over a fixed number of iterations at a large time step. The solution was considered converged if no observable changes could be noted on line plots of several different axial and circumferential surface pressure distributions over a period of 400-500 iterations.

Simulation Conditions

Depending on the altitude and flight velocities involved, complete CFD simulation of jet interaction flowfields can require the use of large sets of finite-rate chemical reactions (dissociated air plus jet species), two-phase flow models (for solid rocket divert motors), and fully-coupled advanced turbulence models. All of these modeling requirements can significantly increase the computational cost of a single solution. As such, when coupled with program resource constraints and the large number of grid points required to resolve the gradients in a jet interaction flow, it is generally not practical to compute large numbers of sc' :ions including finite-rate chemistry or two-phase effects, even on modern vector and parallel supercomputers.

At high altitudes and lower velocities, however, the influence of chemical reactions is generally small and the flow can adequately be treated as a mixture of perfect gases (frozen flow assumption). This approach results in significant computational savings, making the JI problem more tractable, and is the method utilized in this study. Moreover, even for cases where chemistry effects are potentially important, perfect gas simulations have the potential to uncover other important data trends at significantly lower cost.

Two different cases were examined during this study-
(1) a flight simulation at Mach 11 (3.4 km/s), 65 km altitude, $\alpha=+4°$, and
(2) a wind tunnel simulation at Mach 8, Re/m= 2.0 million, $\alpha=+5°$.

For both cases, the jet consists of a single divert thruster located at the vehicle center-of-gravity firing on the leeward side of the vehicle and the approach flow gas is considered to be a calorically perfect gas (air) with a specific heat ratio of $\gamma=1.4$. For the wind tunnel case, the injectant gas is also considered to be perfect gas air and the same model is used for both the approach flow and jet gases.

In the flight simulation, however, so-called "hot jet" effects are included. In this case, the jet gas is considered to be a thermally perfect gas (variable γ) with a molecular weight of approximately 22. The variable γ effects are included by assuming that the injectant gas has three vibrational energy modes (such as might be found in polyatomic molecules like CO_2 and H_2O) each with a characteristic temperature of 1000 K. As a result, at low temperatures, the injectant gas will have $\gamma=1.4$, but at higher temperatures (such as those at jet exit or in the separated region upstream of the jet), it will have a value of $\gamma \approx 1.18$. The injectant gas molecular weight and high temperature specific heat ratios have both been chosen here to be values typical of exit gas mixtures for hydrocarbon fueled thrusters. A comparison of these and other flowfield parameters for the two calculations are presented in Table 1.

As noted earlier, original plans for this study called for CFD simulations at more than one altitude under boosted flight conditions. However, as noted in the next section, no separation was observed onto the vehicle forecone at the highest altitude to be considered (65 km). As such, it was no longer necessary to perform the other simulations at lower altitudes since separation extent has been shown to decrease with increasing freestream dynamic pressure (i.e. lower altitudes at the same velocity).[3, 10]

The wind tunnel case was selected to correspond as closely as possible to the flight condition of interest to provide a reasonable validation calculation. A larger angle-of-attack (5° vs. 4° for the flight case) and smaller momentum flux ratio (2.91 vs. 9.31 for the flight case) were used for the wind tunnel simulation because no discrete measurements were available from the wind tunnel test for the flight values.

Computational Grids

The three-dimensional computational grids for these two computations consist of a 41 x 49 x 153 (circumferential x radial x axial) grid for the flight computation and a similar 41 x 49 x 125 grid for the wind tunnel case. Scaled versions of the same grid could be used for the two computations because the geometry tested in the wind tunnel is a scale model of that used for the flight simulation.

A perspective view of the wind tunnel grid is presented in Figure 2 and a sketch of the vehicle geometry is given in Figure 3. The pictured computational grid was generated using the GRIDGEN suite of codes (version 9.0) available from NASA through COSMIC.[11] Two geometric features of interest in Figure 3 are the location of the divert jet on the aft conic surface and the surface discontinuity which occurs at the forecone/shroud attachment ring juncture.

As shown in Figure 2, the grid is tightly clustered adjacent to the body surface in the radial direction to capture viscous effects. Tight clustering is also employed near the injector exit and at the forecone/shroud attachment ring juncture. Small grid resolution is needed in these areas to adequately capture the large flowfield gradients. Inadequate grid resolution in these areas could lead to excessive numerical smoothing of the separated region causing it to "stall" at the forecone/shroud attachment ring when it should really propagate further upstream onto the forecone. These effects of grid resolution on upstream separation propagation have previously been observed during other similar studies.

The flight grid was formed by adding additional axial grid points near the forecone/shroud attachment ring juncture to the baseline grid used for the wind tunnel study. These points were added as part of a grid convergence study for the flight case. It should be noted that no significant differences in the predicted separation distance occurred between the two grids for the simulated flight condtions.

Results

Computed results for the wind tunnel JI simulation are presented in Figures 4 and 5. Figure 4 presents a plot of flowfield pressure contours over the body and in the base and symmetry planes. Meanwhile, Figure 5 presents a line plot of the surface pressure distributions along the windward and leeward

4

centerlines. Because of the large range of pressures involved, a logarithmic scale is used in both plots to show more details.

As seen in Figure 4, a strong system of shocks and expansions results from the interaction of the jet with the primary stream. A number of patterns are seen here that are normally characteristic of jet interaction flows involving very underexpanded jets (i.e. at large jet to freestream mass or momentum ratios). These patterns include a nearly normal jet bow shock which extends far above the body, strong expansion waves immediately upstream and downstream of the jet exit, and a lambda-like separation shock upstream of the jet bow shock that reaches almost to the nose of the vehicle. In addition, waves from the upstream separation on the leeward (top) side are also seen to "wrap-around" the vehicle and cause a separation shock and associated pressure rise on the windward side just aft of the forecone/shroud attachment ring juncture.

This latter observation is further illustrated in Figure 5. After expanding over the nose (near X/L=0.0), the flow on the windward side attains a relatively steady value until it "spikes" at the forecone/shroud attachment ring juncture, expands further and then is compressed again by the "wrap-around" shock on the aft cone surface. In contrast, on the leeward side, after the flow expands around the nose, it is compressed much closer to the nose (near X/L=0.06) by the leeward separation shock.

Comparison is made in Figure 5 between the calculated separation extent (illustrated by the start of the leeward pressure rise) and the separation distance measured from Schlieren photographs in the wind tunnel test. The CFD solution is seen to exhibit excellent agreement with the data, underpredicting the measured separation extent by 1.5 percent of body length. The excellent level of agreement observed for this case, along with that demonstrated in prior studies, [1] provides confidence in the ability of the code to correctly model jet interaction induced separation for this configuration.

Comparable results for the Mach 11 flight computation are presented in Figures 6 and 7. Figure 6 shows Mach contours in the wind and lee symmetry planes and also in the base plane while Figure 7 presents the windward and leeward centerline surface pressure distributions for this case. Many of the overall features of this computation are qualitatively similar to those observed for the wind tunnel calculation - large plume extent above the body, strong expansion waves near the jet exit, the presence of a lambda-type separation shock upstream of the jet, and the effects of the jet "wrapping-around" the vehicle to cause a separation shock and pressure rise on the windward side of the vehicle. Quantitatively, however, strong differences are observed between the two solutions.

As has already been noted, the extent of the separated region upstream of the jet on the leeward surface (indicated by the shape of the separation shock upstream of the jet) is much smaller for the flight simulation than for the wind tunnel case. In addition, comparison of Figures 4 and 6 shows that the jet bow shock projects further forward and is more curved for the flight case than for the tunnel simulation. These differences in the observed shock shapes (and the resulting surface pressure distributions) are a direct result of differences in the way that the two flowfields respond to the jet disturbance.

More detailed comparison of Figures 5 and 7 illustrates other differences in the two solutions. For example, as also noted in Table 1, the jet to freestream static pressure ratio is nearly an order of magnitude higher for the flight case than for the simulated tunnel conditions. As a result, the flow compression upstream of the jet and the expansion and recompression downstream of the jet are more pronounced in the flight computation because of the stronger local pressure gradients. In addition, the surface pressure downstream of the jet recovers to "freestream-like" values more quickly in the flight simulation.

Factors Influencing Extent of Jet Separation

In order to better understand the reasons for the observed differences in the two presented solutions, it is first useful to discuss what factors influence jet interaction flowfield behavior. In the past, analytical jet interaction studies have often attempted to model the influence of the jet as an equivalent disturbance. Examples of such models include the work of Zukoski and Spaid [12] where the jet momentum is used to define an equivalent disturbance caused by a forward facing axisymmetric body or the work of Broadwell [13] which used blast wave theory and the jet energy to compute the expected jet influence. One important thing which can be gleaned from classical models like these is that the amount of influence the jet has on the flowfield (ie. the extent of the upstream separated region or of changes in the

surface pressure distribution) is directly tied to the size of the jet disturbance. Factors which change the size of the jet disturbance will therefore change the jet influence. It is for this reason that quantities such as jet to freestream mass and momentum flux ratios, kinetic energy (or velocity) ratio, or static and stagnation pressure ratios have often been used to characterize jet interaction flowfields. All of these quantities provide a different means of comparing the size of the jet disturbance.

A comparison of these parameters for the current simulations are presented in Table 1. As shown, the momentum flux, mass flux, static pressure, and kinetic energy ratios are all larger for the flight case than for the wind tunnel case. Larger values of these parameters imply a larger jet disturbance and thus a larger separation distance for the flight case. On the other hand, the lower angle-of-attack for the flight case will tend to reduce the extent of separation. It is not known a priori which of these effects will dominate.

The matter is further complicated by the fact that changes in one flowfield parameter can have competing effects on the size of the jet disturbance. For example, in the flight computation, freestream Mach number is increased, which will result in stronger shocks and stronger expansions relative to the tunnel case. However, although the increased Mach number implies a stronger interaction between the jet and the approach flow, which will tend to increase the extent of separation upstream of the jet, it also implies a stronger expansion over the forecone/shroud ring juncture, which will tend to resist the spread of the separated region onto the forecone.

Similarly, the elevated total temperatures associated with the hot jet cause it to have a higher kinetic energy ratio (or velocity ratio) than the cold jet, but also cause it to have a lower specific heat ratio. The larger kinetic energy ratio would seem to imply a bigger jet disturbance and hence a bigger separated region. On the other hand, the lower ratio of specific heats implies that expansions involving the hot jet will be weaker than those for the cold jet (i.e. the gas with the lower specific heat ratio will expand to a higher pressure ratio for a given turning angle). This last factor was also cited by Dang and Chamberlain [5] as one possible reason for the reduced extent of the low pressure region downstream of the

jet (relative to tunnel computations) which they observed for their flight computations.

For the specific case under study, it appears that the effects of the weaker jet expansions (caused by the lower specific heat ratio for the hot jet), the stronger expansions around the forecone/shroud attachment ring juncture (due to the increased freestream Mach number), and the lower angle-of-attack dominate. The net result of these effects is to halt the upstream progress of the separated region in the flight computation at the forecone/shroud attachment ring juncture and keep it from covering the forecone as it did under tunnel conditions. Nevertheless, it is uncertain how the flight trends would change relative to the wind tunnel results for other Mach numbers, angles-of-attack, jet total temperatures, jet momentum ratios etc.

Based on these observations, it should be clear that care must be taken when attempting to extrapolate wind tunnel jet interaction data to the flight environment. A multitude of factors are involved (Mach number, mass and momentum flux ratios, jet specific heat ratio and total temperature, flight altitude, etc.) which often have competing effects on the anticipated trends.

The results from this study (and others [5,7]) imply that one effective way of predicting flight jet interaction effects is to use cold jet wind tunnel data to validate/calibrate computational models for a particular vehicle geometry. The validated computational model can then be applied at flight conditions to obtain the expected flight behavior. This type of validation/calibration process includes determining such things as grid resolution requirements, establishing confidence in model predictions for the configuration of interest, and obtaining a better understanding of the numerical behavior of the model (robustness, approximate computational time, allowable time step size, approximate number of iterations to convergence, etc.). This combined use of computational and experimental methodologies, when applied carefully, can supply more accurate predictions for jet interaction effects than can either method on its own.

Conclusions

Computational fluid dynamics simulations have been performed for jet interaction flowfields over a

biconic endoatmospheric interceptor under both tunnel and flight conditions. Comparison of the predicted and measured separation lengths for the cold jet wind tunnel case showed excellent agreement, with the separated region upstream of the jet extending almost to the vehicle nose. Flight computations for a hot jet at a higher Mach number and jet to freestream momentum flux ratio showed significantly less separation that did not extend at all onto the forecone.

A number of the factors which influence the behavior of a jet interaction flowfield were subsequently discussed. It was demonstrated that changes in these parameters can often have opposing effects on the flowfield. For the current computations, the reduced size of the flight predicted separated region is attributed to a weaker jet expansion (due to the reduced specific heat ratio associated with the hot jet), a stronger expansion of the approach flow over the forecone/shroud attachment ring juncture (because of the higher approach flow Mach number), and a slightly reduced angle-of-attack. All of these effects tend to reduce the upstream extent of the separated region and keep it from spreading forward onto the forecone.

It is noted that for different conditions (Mach number, angle-of-attack, flight altitude, etc.), very different qualitative trends between tunnel and flight could occur. The results of this study illustrate that better estimates of jet interaction flight performance can be obtained from a combined experimental/computational approach than by either method alone.

References

1. Hudson, D. J. and Trolier, J. W., "Aerothermal and Aero-Optic Performance of a Modified Endoatmospheric Interceptor", SAIC Report No. 94/1052, January 1994.

2. Hudson, D. J. and Trolier, J. W., "Solid Rocket Jet Interaction Effects For a Modified Exoatmospheric Interceptor", Final Report Prepared for BMDO, October 1994.

3. Trolier, J. W. and Hudson, D. J., "Ground Test Capability For Jet Interaction Effects on TMD Interceptor Performance", SAIC Report to BMDO/GST, December 1993.

4. Chan, S.C., Roger, R. P et. al., "Integrated Jet Interaction CFD Predictions and Comparison to Force and Moment Measurements for a Thruster Attitude Controlled Missile", AIAA Paper 93-3522, August 1993.

5. Dang, A. and Chamberlain, R., "Computational Fluid Dynamics Predictions of THAAD Jet Interaction Effect in Tunnel and Flight", Presented at 4th AIAA/BMDO Technology Readiness Conference, Natick, MA, July 1995.

6. Chrusciel, G. T., et.al., "Parametric Wind Tunnel Results of THAAD Kill Vehicle Jet Interaction Effects", Presented at 4th AIAA/BMDO Technology Readiness Conference, Natick, MA, July 1995. (CONFIDENTIAL)

7. Dang, A., et. al., "Analysis of THAAD Jet Interaction Parameters for Low Endoatmospheric Flight", Presented at 5th AIAA/BMDO Technology Readiness Conference, Fort Walton Beach, FL, September 1996. (SECRET)

8. Harvey, D. W., Davis, J. C., and Timmer, H., "Control Forces and Moments Produced by Large Lateral Jets on a Hypersonic Biconic Vehicle", MDAC Report H 1642, October 1984. (CONFIDENTIAL)

9. McGrory, W. D., Slack, D. C., Applebaum, M. P, and Walters, R. W., "GASP Version 2.0, User's Manual", Aerosoft Corporation, 1992.

10. High Altitude Maneuver Control (HAMC) Wind Tunnel Test Surface Pressure Data, Computer Printout from NSWC, 1984.

11. Steinbrenner, J. P. and Chawner, J. R., "The GRIDGEN Version 9 Multiple Block Grid Generation Software", MDA Engineering Report 94-01, January 1996.

12. Zukoski, E. E. and Spaid, F. W., "Secondary Injection of Gases Into a Supersonic Flow", AIAA Journal Vol. 2, No. 10, October 1964.

13. Broadwell, J. E., "Analysis of the Fluid Mechanics of Secondary Injection for Thrust Vector Control", AIAA Journal, Vol. 1, No. 5, May 1963.

Table 1 - Parameters Affecting Jet Induced Separation Length

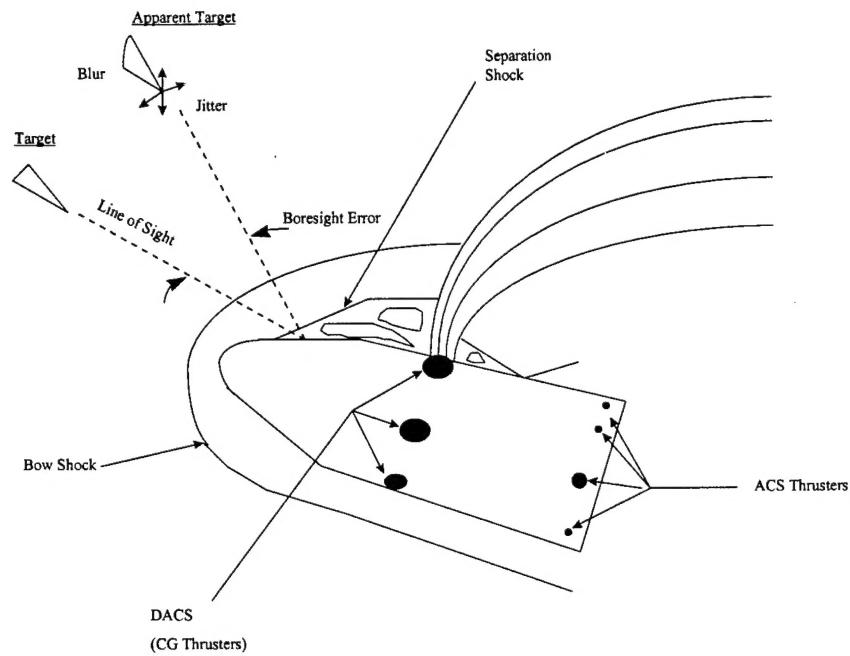| Parameter	Wind Tunnel	Flight
Momentum Flux Ratio $\rho_{jet} V_{jet}^2 A_{jet} / \rho_\infty V_\infty^2 A_{ref}$	2.91	9.31
Mass Flux Ratio $\rho_{jet} V_{jet} A_{jet} / \rho_\infty V_\infty A_{ref}$	5.44	12.21
Static Pressure Ratio P_{jet} / P_∞	738.4	5651
Kinetic Energy Ratio V_{jet}^2 / V_∞^2	0.285	0.5804
Angle-of-Attach (degrees)	5.0	4.0
Freestream Mach Number M_∞	8.0	11.0
Ratios of Specific Heats $\gamma_{jet}, \gamma_\infty$	$\gamma_{jet} = \gamma_\infty = 1.4$	$\gamma_\infty = 1.4$ $\gamma_{jet} \approx 1.18$

Figure 1 - Schematic of Jet Interaction Induced Aero-Optic Effects For Forward Looking Endoatmospheric Interceptors
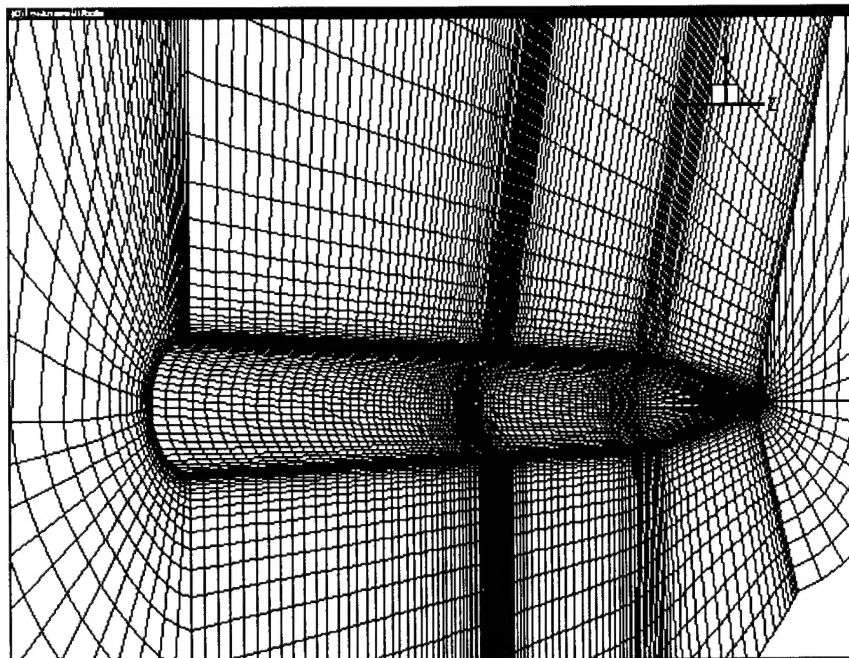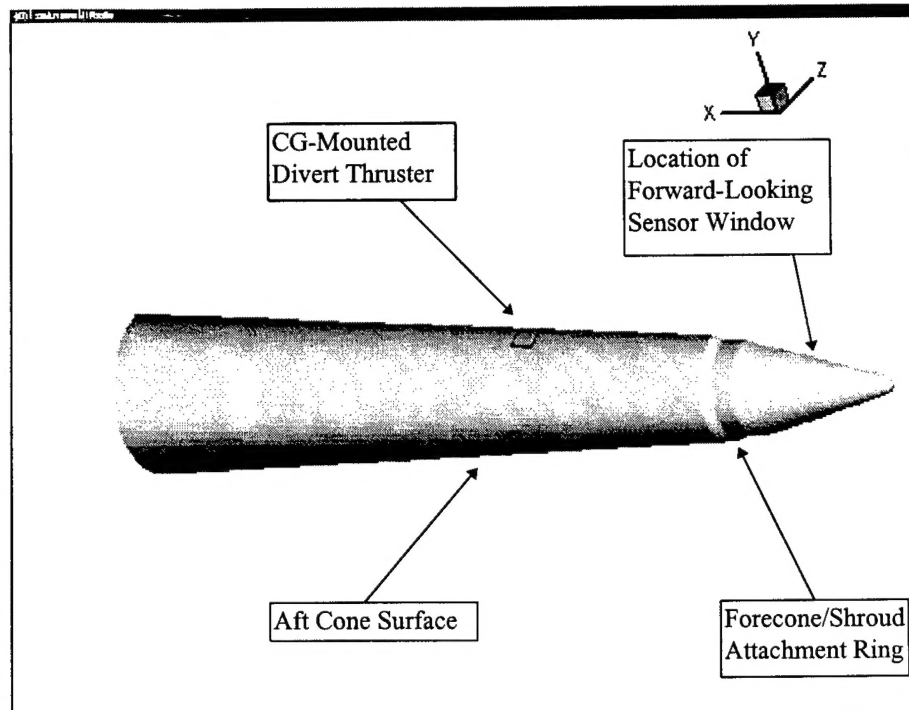

Figure 2 - Computational Grid for Jet Interaction Calculations
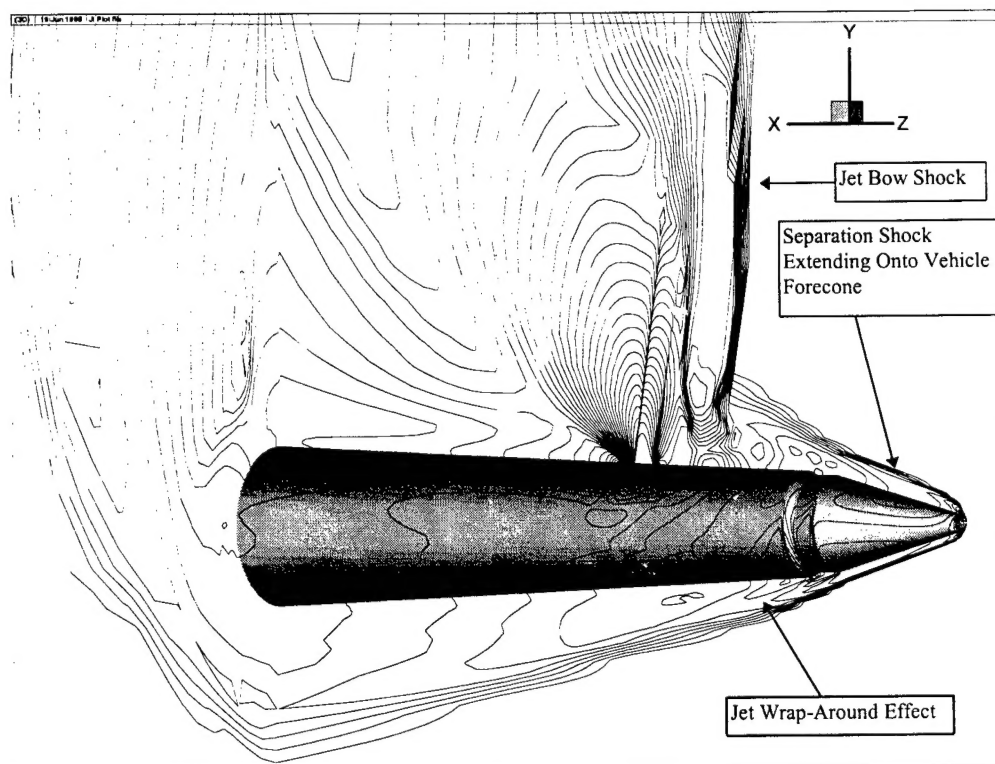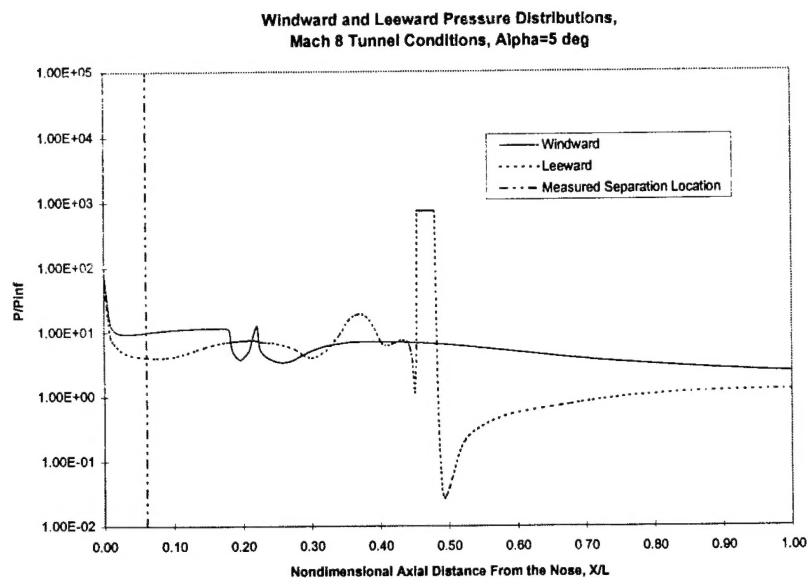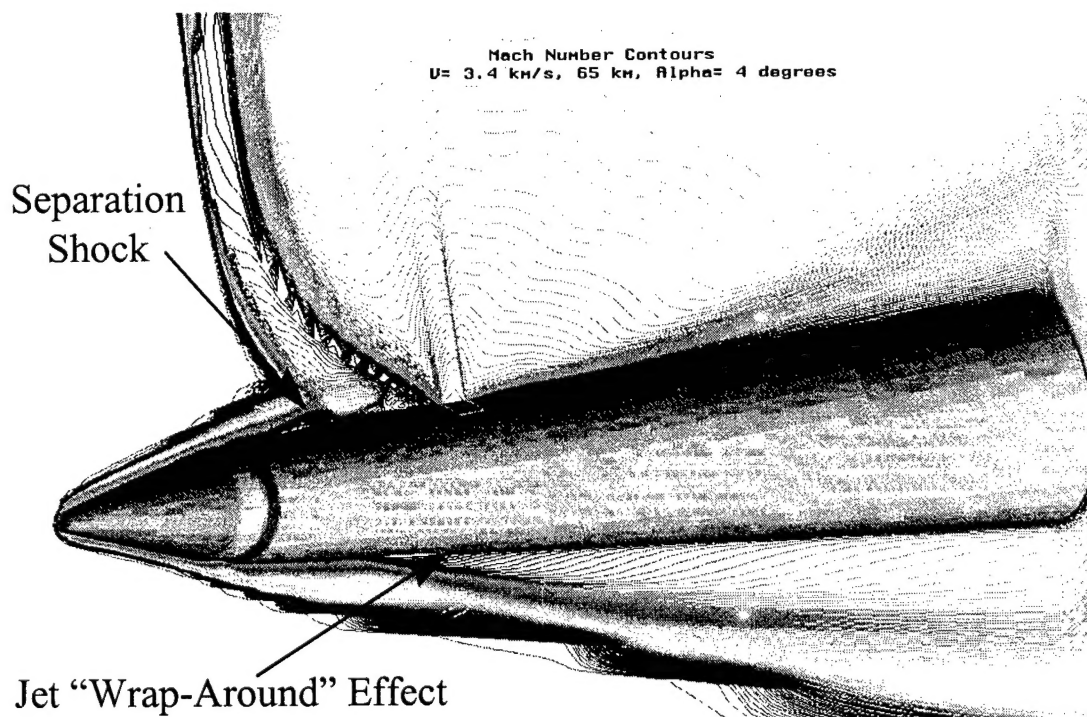
Figure 3 - Interceptor Geometry

Figure 4 - Surface Pressure Contours (Logarithmic Scale)
Wind Tunnel Test Simulation, M=8.0, Re/m = 2.0E6, α= 5°

Figure 5 - Comparison of Predicted and Measured Separation Lengths, Windward and Leeward Surface Pressure Distributions, Wind Tunnel Case, M=8.0, Re/m = 2.0E6, $\alpha = 5^o$

Figure 6 - Mach Number Contours, Flight Case Simulation V= 3.4 km/s (Mach 11), Altitude = 65 km, $\alpha= 4^o$

Windward and Leeward Pressure Distributions,
Alpha=4 deg, h= 65 km, Vinf= 3.4 km/s
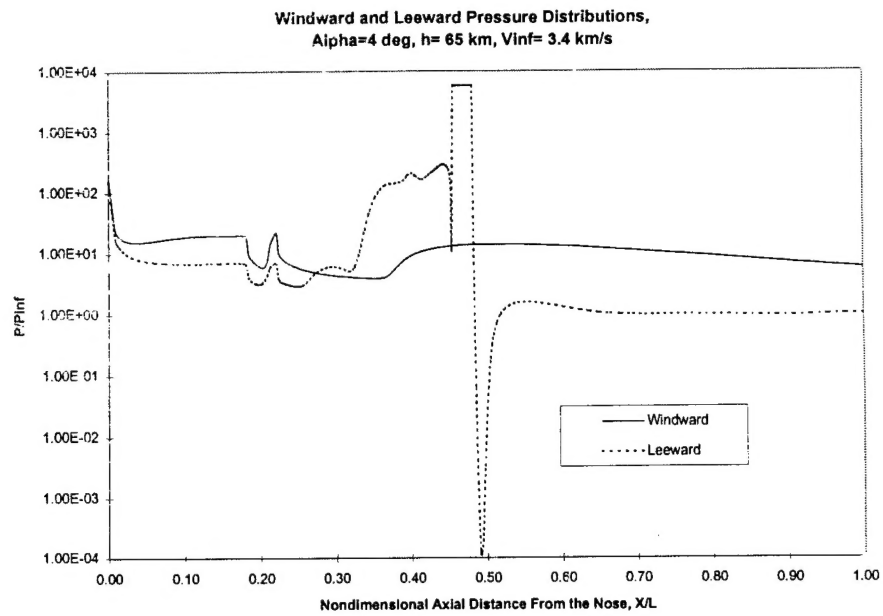
Figure 7 - Windward and Leeward Surface Pressure Distributions,
Flight Case Simulation, V= 3.4 km/s (Mach 11), Altitude = 65 km, α= 4°

Title of Document ___Hot Jet and Mach Number Effects on___
___Jet Interaction Upstream Separation___

PLEASE CHECK THE APPROPRIATE BLOCK BELOW:

☒ ___1___ copies are being forwarded. Indicate whether Statement A, B, C, D, E, F, or X applies.

☒ DISTRIBUTION STATEMENT A:
   APPROVED FOR PUBLIC RELEASE: DISTRIBUTION IS UNLIMITED

☐ DISTRIBUTION STATEMENT B:
   DISTRIBUTION AUTHORIZED TO U.S. GOVERNMENT AGENCIES
ONLY: (Indicate Reason and Date). OTHER REQUESTS FOR THIS
DOCUMENT SHALL BE REFERRED TO (Indicate Controlling DoD Office).

☐ DISTRIBUTION STATEMENT C:
   DISTRIBUTION AUTHORIZED TO U.S. GOVERNMENT AGENCIES AND
THEIR CONTRACTORS; (Indicate Reason and Date). OTHER REQUESTS
FOR THIS DOCUMENT SHALL BE REFERRED TO (Indicate Controlling DoD Office).

☐ DISTRIBUTION STATEMENT D:
   DISTRIBUTION AUTHORIZED TO DoD AND U.S. DoD CONTRACTORS
ONLY; (Indicate Reason and Date). OTHER REQUESTS SHALL BE REFERRED TO
(Indicate Controlling DoD Office).

☐ DISTRIBUTION STATEMENT E:
   DISTRIBUTION AUTHORIZED TO DoD COMPONENTS ONLY; (Indicate
Reason and Date). OTHER REQUESTS SHALL BE REFERRED TO (Indicate Controlling DoD Office).

☐ DISTRIBUTION STATEMENT F:
   FURTHER DISSEMINATION ONLY AS DIRECTED BY (Indicate Controlling DoD Office and Date) or HIGHER
DoD AUTHORITY.

☐ DISTRIBUTION STATEMENT X:
   DISTRIBUTION AUTHORIZED TO U.S. GOVERNMENT AGENCIES
AND PRIVATE INDIVIDUALS OR ENTERPRISES ELIGIBLE TO OBTAIN EXPORT-CONTROLLED
TECHNICAL DATA IN ACCORDANCE WITH DoD DIRECTIVE 5230.25. WITHHOLDING OF
UNCLASSIFIED TECHNICAL DATA FROM PUBLIC DISCLOSURE. 6 Nov 1984 (Indicate date of determination).
CONTROLLING DoD OFFICE IS (Indicate Controlling DoD Office).

☐ This document was previously forwarded to DTIC on _____ (date) and the
AD number is _____.

☐ In accordance with provisions of DoD instructions. the document requested is not supplied because:

☐ It will be published at a later date. (Enter approximate date. if known).

☐ Other. (Give Reason)

**DoD Directive 5230.24, "Distribution Statements on Technical Documents," 18 Mar 87, contains seven distribution statements, as
described briefly above. Technical Documents must be assigned distribution statements.**

Douglas J. Hudson
Print or Type Name

(610) 687-4440
Telephone Number

Authorized Signature/Date